Geochemistry, Geophysics, Geosystems®

AGU ADVANCING EARTH AND SPACE SCIENCES

RESEARCH ARTICLE
10.1029/2023GC011105

Correspondence to:
M. van der Does,
mdoes@awi.de

Late Holocene Dust Deposition Fluxes Over the Entire South Atlantic Ocean

Michèlle van der Does[1] , Frank Lamy[1] , Stephan Krätschmer[1] , Jan-Berend W. Stuut[2,3] , Christoph Völker[1] , Martin Werner[1] , Roseanne Schwarz[4], Marty Fleisher[4], and Gisela Winckler[4,5]

[1]Alfred Wegener Institute, Helmholtz Centre for Polar and Marine Research, Bremerhaven, Germany, [2]NIOZ, Royal Netherlands Institute for Sea Research, Texel, The Netherlands, [3]Faculty of Science, Department of Earth Sciences, Vrije Universiteit Amsterdam, Amsterdam, The Netherlands, [4]Lamont-Doherty Earth Observatory, Columbia University, Palisades, NY, USA, [5]Department of Earth and Environmental Sciences, Columbia University, New York, NY, USA

Abstract Mineral dust accumulated on the ocean floor is an important archive for reconstructing past atmospheric circulation changes and climatological conditions in the source areas. Dust emitted from Southern Hemisphere dust sources is widely deposited over the oceans. However, there are few records of dust deposition over the open ocean, and a large need for extended geographical coverage exists. We present a large data set (134 surface sediment samples) of Late Holocene dust deposition from seafloor surface sediments covering the entire South Atlantic Ocean. Polymodal grain-size distributions of the lithogenic fraction indicate that the sediments are composed of multiple sediment components. By using end-member modeling, we attempt to disentangle the dust signal from non-aeolian sediments. Combined with [230]Th-normalized lithogenic fluxes, we quantified the specific deposition fluxes for mineral dust, crrent-sorted sediments and ice-rafted debris (IRD). Although the method could not completely separate the different components in every region, it shows that dust deposition off the most prominent dust source for the South Atlantic Ocean—southern South America— amounts up to approximately 0.7 g cm^{-2} Kyr^{-1} and decreases downwind. Bottom-current-sorted sediments and IRD are mostly concentrated around the continental margins. The ratio of the coarse to fine dust end members reveals input from north African dust sources to the South Atlantic. The majority of the observations are in good agreement with new model simulations. This extensive and relevant data set of dust grain size and deposition fluxes to the South Atlantic could be used to calibrate and validate further model simulations.

Plain Language Summary Ocean records of mineral dust can be used to reconstruct past climatic changes such as wind strength and aridity in the source regions, and also marine biological productivity. However, in the remote open ocean, dust samples are difficult to obtain and therefore records are sparse. We present a large data set of dust deposition, determined from the top centimeter of ocean floor sediments, covering the entire South Atlantic Ocean. These appeared to be complex mixtures of different sediment types, which we attempted to unmix mathematically. This resulted in four individual components, which are fine and coarse mineral dust, current-sorted sediments and ice-rafted debris (IRD). Although the unmixing has its limitations, it shows that the dust deposition off the most prominent dust source for the South Atlantic Ocean— southern South America—is significant and decreases downwind as dust settles during transport across the ocean. Current-sorted sediments and IRD are mostly concentrated around the continental margins. The results also reveal dust transport across the equator from north African dust sources and show similarities with new model simulations. This extensive and relevant data set of dust grain size and deposition fluxes to the South Atlantic can be used to calibrate and validate further model simulations.

1. Introduction

Mineral dust is a major component of sediment input to the remote open ocean. Annually, about 2,000 Tg of dust is emitted from dust sources worldwide, of which 25% is deposited into the oceans (Shao et al., 2011). In sedimentary archives, including deep-sea sediment cores, dust fluxes and particle size can serve as paleo-climate indicators for conditions such as source aridity, wind strength and wind direction (McGee et al., 2013; Rea, 2007). Dust flux and particle size of deposited dust are also affected by the distance they have traveled, with more and coarser-grained dust being deposited closer to the sources (Rea, 2007; van der Does, Brummer, et al., 2021; van der Does et al., 2016). Closer to the continents, riverine sediments have become the main contributor to oceanic
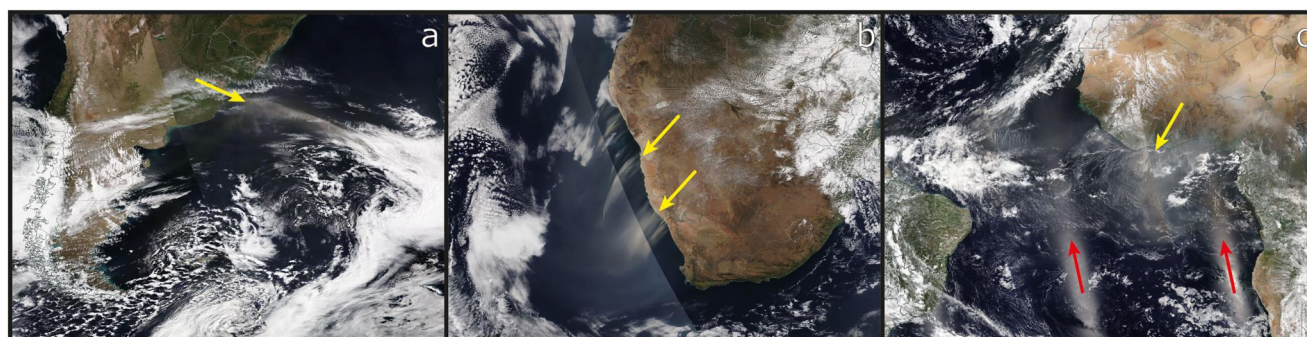
Figure 1. Modern dust deposition off southern South America (a), southern Africa (b) and interhemispheric transport from northern Africa across the Equator (c), where the dust plumes are indicated by the yellow arrows. The red arrows in (c) show the sun's reflection on the ocean surface captured by the satellite. Images from NASA Worldview Corrected Reflectance (True Color) NOAA-20/VIIRS, of 25 October 2021 (a), 27 June 2022 (b), and 1 February 2022 (c).

sediments (Rea, 2007). The most and largest dust sources are on the Northern Hemisphere, which produce up to an order of magnitude more dust than Southern Hemisphere sources (Prospero et al., 2002; Rea, 1994).

Mineral dust has several direct and indirect impacts on climate. Atmospheric dust influences the radiation budget through scattering and absorbing solar radiation (Arimoto, 2001) and acts as cloud condensation and ice nuclei (Twohy et al., 2009). In addition, soluble iron-rich dust deposition affects marine biological productivity and the global carbon cycle through iron fertilization of high nutrient low chlorophyll regions (Duce et al., 1991; Martin, 1990). Antarctic ice cores have recorded dust deposition over multiple glacial cycles, and these records reveal a ~25-fold increase in dust deposition during glacial periods compared with interglacial periods (Lambert et al., 2008). Paleoceanographic reconstructions found that iron fertilization through dust input in the Subantarctic Zone of the Southern Ocean can explain up to 40 ppmv of the atmospheric CO_2 decrease observed during glacial periods (Martínez-García et al., 2014).

Model simulations show that about 10% of all global dust emissions come from Southern Hemisphere sources (Kok et al., 2021b; Li et al., 2008). These simulations revealed that dust transport (<20 μm) over the Southern Hemisphere mainly comes from sources including South America (~190 Tg a^{-1}), Australia (~160 Tg a^{-1}), southern Africa (~100 Tg a^{-1}), New Zealand, as well as inter-hemispheric transport from the Northern Hemisphere, mainly from North Africa (Kok et al., 2021b; Neff & Bertler, 2015). The main carriers of dust from these Southern Hemisphere sources are the southern westerly winds (SWW). Transport from southern African sources is weak since these are more remote from the influence of the westerlies, but are rather transported by the southeast trade winds (Dupont & Wyputta, 2003; Shi et al., 2001; Stuut et al., 2002). Therefore, their influence at high Southern latitudes is relatively small.

Average estimations from model simulations 68% of dust deposition to the South Atlantic reveal that about 68% originates from South-American sources, 24% from Southern Africa, and minor inputs (~4%) from Northern Hemisphere sources (Figure 1; Kok et al., 2021b). The main South-American dust sources include Patagonia, an area of over 900,000 km², extending from 39°S to the southernmost tip of the continent; central-western Argentina, a ~600,000 km² area extending from the eastern flank of the Andes to the western slope of the Sierras Pampeanas; and the Puna-Altiplano Plateau, which is a 1,000 by 200 km basin located in the central Andes ~4,000 m asl (Gili et al., 2017; Prospero et al., 2002). Dust from Patagonia has been traced to the free troposphere in the Sub-Antarctic Atlantic Ocean, where it is quickly diluted by removal processes over the ocean (Gassó & Stein, 2007). Dust concentrations of South American sources are found to decrease sharply downwind and eastward, with one order of magnitude decrease upon reaching the eastern margin of the Atlantic Ocean near South Africa (Li et al., 2008).

In southern Africa, the main dust sources include the Makgadikgadi Depression in the lowest part of the Kalahari Desert in Botswana, and the Etosha Pan in northern Namibia (Li et al., 2008; Prospero et al., 2002), but also several coastal sources in Namibia from which the dust is transported toward the South Atlantic Ocean with strong Berg winds (Gili et al., 2022). Dust emitted from southern African sources is not transported as far south as from South American sources due to less efficient dust-transporting winds and therefore has a limited influence on the Southern Ocean and Antarctica (Neff & Bertler, 2015). Dust transport from Australian sources to the South

Atlantic is mostly blocked by the Andes Mountains in South America and therefore only has a minor contribution (Li et al., 2008). Dust from Northern Hemisphere sources is also transported across the equator, although in very small quantities and therefore contributes little to deposition in the South Atlantic (Kok et al., 2021b; Li et al., 2008). Much of these data come from modeling studies, indicating the need for direct observational data in this vast region.

Latest estimates from model simulations of annual dust (<20 μm) deposition in the South Atlantic range between 51 and 149 Tg (Kok et al., 2021b), of which the majority is deposited by wet-depositional processes (Duce et al., 1991; Li et al., 2008). This is in agreement with findings by Gaiero et al. (2003), who estimated that ∼30 Tg of Patagonian dust is deposited in the South Atlantic, as well as ∼40 Tg of sediments from coastal erosion and ∼2 Tg of riverine sediments. Model simulations by Johnson et al. (2010) estimate a yearly Patagonian dust emission flux of ∼30 Tg and a deposition of 22 Tg to the South Atlantic Ocean for dust particles up to 12 μm. Wet deposition is found to be the primary removal mechanism, accounting for 40% and 80% of total deposition near the coast and over the open ocean, respectively (Johnson et al., 2010).

In addition to aeolian sediments, lithogenic material can also be delivered to and transported within the Atlantic and the Southern Ocean by surface and deeper ocean currents such as the Atlantic Circumpolar Current flowing eastward throughout the Southern Ocean following SWW, the Weddell Gyre, the Agulhas Current and Benguela Current around southern Africa, and the Brazil Current flowing south along South America, as well as bottom currents of Antarctic Bottom Water and Circumpolar Deep Water (Figure 2).

Records of dust deposition over the open ocean are sparse. Climate models can contribute to this by simulating the dust deposition over these remote areas over recent and palaeo-timescales, but these models seem to underestimate the dust deposition compared to fluxes obtained from sediment records. This has been attributed to inaccurate representation of (very) coarse dust particles in model simulations (Adebiyi & Kok, 2020). Large discrepancies in the existing measurements also indicate the need for an expanded geographical coverage of direct observations of dust deposition in the oceans. This will contribute to validate model simulations and satellite observations.

Here, we present grain-size measurements and ^{230}Th-normalized lithogenic fluxes of seafloor surface sediments covering the entire South Atlantic Ocean, which will form an important data set of direct observations of dust deposition over such a vast region. ^{230}Th-normalized ^{232}Th fluxes are often used as a proxy for dust fluxes in the open ocean (Winckler et al., 2008, 2016). In places along continental margins with additional lithogenic input, such as riverine, ice-rafted sediments or current-transported sediments, ^{232}Th-based lithogenic fluxes of dust deposition may be an overestimation (Diekmann et al., 2003; Ouyang et al., 2021). We propose an individual characterization of different sediment fractions contributing to the total lithogenic flux, which is achieved by end-member (EM) modeling of grain-size distributions. This results in more specific fluxes for fine-grained and coarse-grained dust, in addition to current-sorted sediments as well as ice-rafted debris (IRD).

2. Material and Methods

2.1. Sample Material

A total of 134 surface sediments from the ocean floor from multiple expeditions with *FS Polarstern* and *FS Meteor*, obtained between 1988 and 2005 in the South Atlantic Ocean, were analyzed (Figure 2). Detailed information on the samples is provided in Table S1. Most samples were taken by a multicorer and some by a giant box corer. To avoid large contributions from hemipelagic and riverine sediments, the samples were selected to be >300 km away from the African and South American coasts, following the strategy outlined by Kienast et al. (2016). This was not the case for samples close to the Antarctic continent. Since sedimentation rates in the Atlantic Ocean are on the order of a few centimeters per thousand years, each sample represents several hundreds of years of sediment accumulation and dust deposition (Stuut & Lamy, 2004). For the few samples for which dating was available, most ages ranged between 0.23 and 0.44 ka BP, with two samples dated to 2.3 and 2.69 ka BP (Table S1), and therefore represent the Late Holocene.

2.2. Grain-Size Analysis

Prior to grain-size analysis, the lithogenic fraction was isolated by removing the biogenic components chemically. About 200–500 mg of the bulk freeze-dried sediments were weighed into 50 mL centrifuge tubes. First, organic
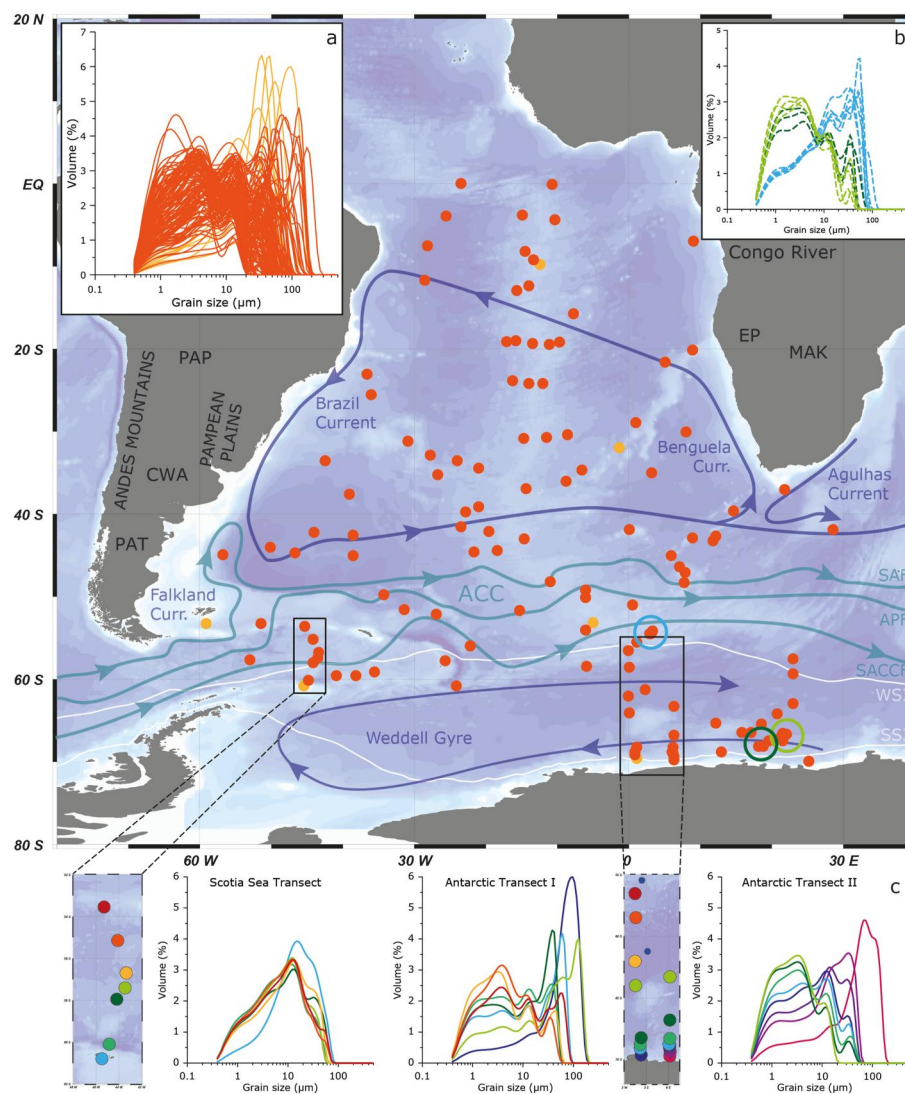
Figure 2. Map with locations of the surface samples from the South Atlantic Ocean. Outliers marked in light orange (see text). (a) Grain-size distributions of all samples (*N* = 134). Solid lines show main surface ocean currents, based on Diekmann et al. (2003) and Peterson and Stramma (1991), mean positions of major front systems (Orsi et al., 1995), and mean extent of sea ice (Comiso, 2003). SAF, Subantarctic Front; APF, Antarctic Polar Front; SACCF, Southern Antarctic Circumpolar Current Front; WSI, winter sea ice; SSI, summer sea ice; ACC, Antarctic Circumpolar Current. The map was generated using Ocean Data View (Schlitzer, 2018). Main dust source regions: PAP, Puna-Altiplano Plateau; CWA, central-western Argentina; PAT, Patagonia; EP, Etosha Pan; MAK, Makgadikgadi Depression. (b) Clustered grain-size distributions of samples marked with colored circles in (a). (c) Highlighted transects and their grain-size distributions.

matter was removed by adding 5 mL H_2O_2 (35%) and the samples were placed in a hot water bath at 100°C for ~1–2 hr until the reaction stopped, adding small amounts of demineralized water to prevent the samples from overflowing and also from boiling dry. The samples were then filled with demineralized water and subsequently centrifuged, after which the overlying water was decanted using a water-jet pump. This rinsing was repeated multiple times until the pH was neutral or similar to the demineralized water. Carbonates were removed from the sediments by adding 5 mL HCl (10%). Since the reaction was immediate and complete, the samples were not heated during this step but rather agitated using a vortexer, and subsequently rinsed and centrifuged until the pH was neutral. As a final step, biogenic opal was removed with 15 mL NaOH (20%), and the samples were placed in a hot water bath at 100°C for 3 hr, after which the samples were rinsed and centrifuged until the pH was neutral. Smear slides of a selection of samples were made and a visual inspection using a light microscope ensured the complete removal of all biogenic components prior to further analyses.

Grain-size analyses were performed using a Beckman Coulter laser diffraction particle sizer LS13 320 equipped with a micro liquid module at the Royal Netherlands Institute for Sea Research (NIOZ). Directly prior to grain-size analysis, 2 mL of $Na_4P_2O_7 \cdot 10H_2O$ (sodium pyrophosphate) was added to each sample and sonicated for a few minutes to completely break up the aggregates that may have formed despite the previous chemical treatment. Degassed water was used during analysis to minimize the influence of gas bubbles, and a magnetic stirrer homogenized the sample during analysis. This resulted in particle-size distributions divided into 92 size classes ranging from 0.375 to 2,000 μm. Experiments with internal glass-bead standards reveal the reproducibility to be better dan 0.7 and 0.6 μm for the mean and median particle size (1σ), respectively, and the average standard deviation integrated over all size classes is better than 4 vol.% (van der Does et al., 2016).

2.3. End-Member Modeling

The lithogenic fraction contains, besides mineral dust, other sediment sources including IRD, riverine sediments and hemipelagic sediments transported by (bottom) currents, as is illustrated by their highly unsorted and polymodal grain-size distributions (Figure 2a). In addition, the mineral dust deposited in the South Atlantic can have different continental sources, such as South America and southern Africa, but also Northern-Hemispheric dust sources. Since these all have overlapping grain sizes, they cannot be physically separated from each other, and therefore a mathematical model is used to separate the different base components. Several algorithms are available, so-called EM models, which unmix the grain-size distributions into sedimentologically meaningful components (Weltje, 1997). A comparative study using artificial and published data sets revealed that the results of the program AnalySize for MATLAB (Paterson & Heslop, 2015) are most accurate compared to other EM models (van Hateren et al., 2018). AnalySize was primarily, but not exclusively, designed to unmix grain-size data obtained by laser-diffraction particle-size analyzers.

Weltje and Prins (2007) provide a discussion on the difference between parametric EM modeling (or curve fitting), where the end members are assumed to have unimodal distributions and non-parametric EM modeling, where the shape of the end members is not pre-defined and can reflect polymodal grain-size distributions. The latter proved to be better suited to reconstruct and reflect the mixing of different sediment types (related to provenance) and the unmixing by sedimentary processes and deposition for better interpretation of the geological context. McGee et al. (2013), on the other hand, argue for the parametric method, although a good fit between model and data does not guarantee its aptitude of explaining the underlying geological processes (Weltje & Prins, 2007).

For the purpose of unmixing the observed polymodal grain-size distributions of the samples, we performed the non-parametric EM analysis using AnalySize v.1.1.2 using a non-parametric EM correlation. This method identifies covarying components and reveals information about mixing dynamics or non-selective physical processes and is based on non-negative matrix factorization (Paterson & Heslop, 2015). The EM analysis was performed on 128 of the grain-size distributions after removing 6 outliers (marked in light orange in Figure 2a). The grain-size distributions of these outliers differ much from the rest of the data set so that they influenced the outcome of the basic components of the sediments, and were therefore left out of this reconstruction. End members were calculated for 2–7 EM scenarios (Figure 3).

Up to four EMs show a clear increase in the linear correlation between the data and the EM reconstruction ($R^2 = 0.97$; Figure 3). For the scenarios with five or more EMs, the linear correlation shows a much smaller increase, and more principal components would over-complicate the interpretation of the mechanisms behind the sediment's grain-size distributions, as seen from the EM grain-size distributions.

The 3-EM scenario likely has too few EMs, which is also shown by their polymodal grain-size distributions, indicating additional subpopulations. For the 4-EM scenario, the grain-size distributions are more uniform except the coarsest EM, which would fit well to the characteristic unsorted nature of IRD. In the 5-EM scenario, the two coarsest EMs show such unsorted grain-size distributions indicative of IRD. In the case of our data set, where we are primarily interested in the mineral dust fractions, having two separate IRD EMs would only complicate the interpretation of the results further. Given the nature of the sediments, the possible sediment sources and transport mechanisms, we find that the four-EM scenario would best describe the variability in our data set. These EMs 1–4 have a modal grain size of 1.7, 10.4, 34.6, and 72.9 μm, respectively. The angular deviation between the data and EM reconstruction (theta) equals 6.69 for the 4-EM scenario, and the correlation between the different EMs (EM R^2) equals 0.03.
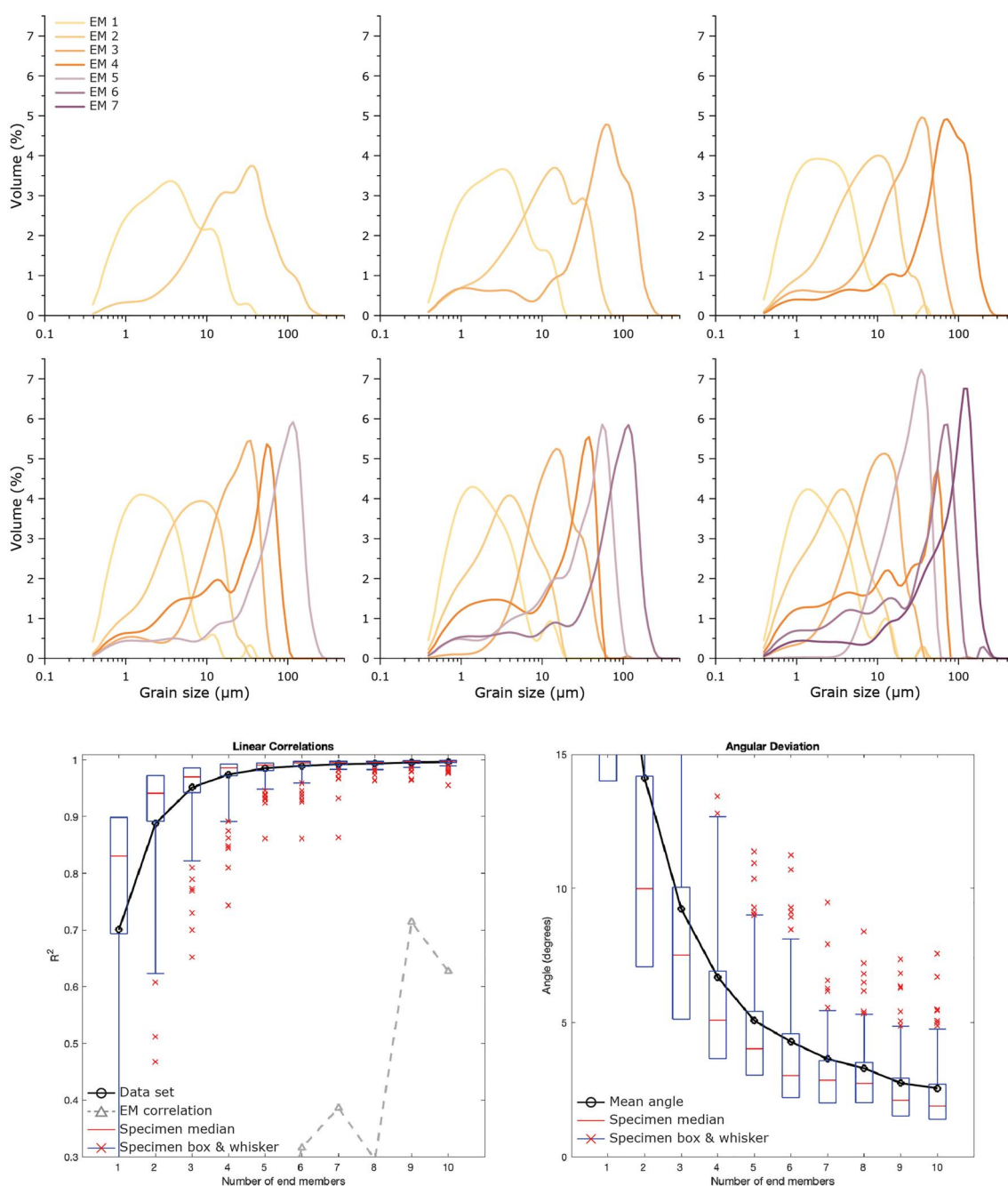
Figure 3. End-member (EM) grain-size distributions for 2–7 EM scenarios (top graphs) and statistics (bottom graphs). The linear correlation (R^2; black line) indicates the fit between the data and the EM reconstruction, while the EM correlation (EM R^2; gray dashed line) shows the linear (in)dependence of the EMs. The angular deviation (theta) represents the angular deviation between the data and EM reconstruction. A low linear correlation and high angular deviation are an indication of a poor fit. A high EM R^2 value indicates that the data are over-fitted and the number of EMs should be reduced.

2.4. Lithogenic Fluxes by [230]Th-Normalization

A total of 134 samples were analyzed for U/Th isotopes on a Thermo Scientific Element 2 ICP-MS at LDEO. Sample preparation utilized a similar procedure to that of Fleisher and Anderson (2003). Briefly, aliquots of about 100 mg of freeze-dried bulk sediment samples were weighed and spiked with a [236]U-[229]Th solution. Subsequently, the samples were completely digested with a mixture of concentrated nitric acid (HNO_3), perchloric acid ($HClO_4$), and hydrofluoric acid on a hot plate. U/Th purification was achieved via Fe-coprecipitation and anion

exchange chromatography. Each batch contained a procedural blank, and blank levels were subtracted from the final isotope values. The average reproducibility of 11 replicates was 7%. This variability between replicates is small relative to the differences between samples. In order to quantify reproducibility, an internal sediment standard (VOICE Internal MegaStandard, or VIMS) was run in each batch, with a maximum difference of 2.2% for ^{230}Th and 7.4% for ^{232}Th ($n = 4$).

We apply the ^{230}Th normalization method to constrain vertical fluxes of sedimentation (for a complete review, see Francois et al., 2004; Costa et al., 2020). This method allows to separate the vertical rain rate of sediments from lateral fluxes into or away from the sample site (i.e., sediment redistribution). Briefly, ^{230}Th is produced in the water column by α-decay from its parent ^{234}U with a half-life of 75,584 ± 110 years (Cheng et al., 2013). ^{230}Th is quickly scavenged and has a very short residence time in the water column and therefore a limited extent of lateral transport (Costa et al., 2020; Francois et al., 2004). The ^{230}Th normalization method, originally proposed by Bacon (1984) and increasingly adopted by the paleoceanography community, is based on the assumption that the flux of scavenged ^{230}Th reaching the seafloor is equal to the well-known production of ^{230}Th in the overlying water column. Since the production rate of ^{230}Th is uniform, the measured concentration of ^{230}Th (corrected for detrital input and decay through time—excess ^{230}Th or ^{230}Th$_{xs0}$) in a sediment sample can be used to determine an instantaneous vertical sediment rain rate. The excess ^{230}Th flux is calculated following the method described by Costa et al. (2020), correcting for the lithogenic ^{230}Th activity, using the lithogenic ^{238}U/^{232}Th ratio of 0.6 ± 0.1 for the Atlantic Ocean (Henderson & Anderson, 2003). No large differences in absolute values for the ^{232}Th-derived lithogenic flux exist when a lithogenic ^{238}U/^{232}Th ratio of 0.4 ± 0.1 for the Southern Ocean is used instead as well as for the spatial trends (maximum 1.85 g cm^{-2} Kyr^{-1} difference for the individual samples). Therefore, we chose the value for the Atlantic Ocean (0.6 ± 0.1) as the most appropriate for our South-Atlantic set of samples. Since the samples represent the top centimeter of the seafloor sediments, we assumed a sediment age of 0 Kyr for the above calculations. Indeed, published ages for the used samples mostly indicate ages well below 1 Kyr (Table S1). In addition, ^{230}Th-normalized fluxes are relatively insensitive to age-model errors (<1% flux error for 1 Kyr age error) (Costa et al., 2020).

The sediment mass accumulation rates (MAR) derived from ^{230}Th are then calculated as follows:

$$\text{Mass Flux}_{230\text{Th}} = \frac{\beta * z}{A_{230\text{Thxs0}}} \tag{1}$$

where β is the production rate of ^{230}Th in the water column (2.562 * 10^{-5} dpm cm^{-3} Kyr^{-1}) by radioactive decay of ^{234}U (Costa et al., 2020), z is the water depth in cm, and A$_{230\text{Thxs0}}$ is the ^{230}Thxs activity at the time of initial sediment deposition.

While the rare isotope ^{230}Th allows estimates of sediment MAR, common Thorium (^{232}Th) can be used as a proxy for terrestrial input to the ocean (Kienast et al., 2016; McGee et al., 2016; Noble et al., 2012; Winckler et al., 2008, 2016). The concentration of ^{232}Th in continental sources is found to be quite consistent across a range of locations, with an average concentration for the upper continental crust of 10.7 ppm (Taylor & McLennan, 1995). By analyzing fine-grained aeolian dust samples, McGee et al. (2016) found a systematic grain-size effect, showing increasing ^{232}Th concentrations with decreasing grain size. They recommend an average ^{232}Th concentration for fine-grained aeolian dust (<5 μm) of 14 ± 1 ppm. Since our main aim is reconstructing mineral dust fluxes over the ocean and since most of mineral dust, especially after long-range transport, consists of particles <5 μm (Kok et al., 2021a), we have used this recommended concentration of 14 ± 1 in our calculations. Using the measured ^{232}Th concentration [^{232}Th], ^{232}Th-derived lithogenic fluxes were calculated as follows (Costa et al., 2020):

$$\text{Lithogenic flux} = \frac{[^{232}\text{Th}] * \text{Mass Flux}_{230\text{Th}}}{14} \tag{2}$$

In the following text, we refer to the ^{230}Th-normalized fluxes of lithogenic ^{232}Th in short as lithogenic fluxes.

2.5. Model Simulations of South Atlantic Dust Deposition

New model simulations by Krätschmer, van der Does, et al. (2022) were compared to the observed dust deposition fluxes over the South Atlantic Ocean. Here we summarize how these simulations were performed.

The simulations are based on pre-industrial climate (1850–1880 CE), with a prior spin-up time of 10 years. The setup consists of the general circulation atmosphere model ECHAM6.3 fully coupled to the aerosol model HAM2.3. Monthly resolved 30-year means for the years 1870–1899 of sea surface temperatures and sea ice concentration are prescribed based on the latest AMIP II data set (Durack & Taylor, 2019).

The spatial resolution of the model is 1.875° × 1.875°, which corresponds to grid cells of approximately 180 km at the equator. In order to compare these simulations to the observed data, the simulated values are linearly interpolated in the grid cells at the according to coordinates. In the vertical, the model consists of 47 layers up to a model height of approximately 80 km (0.01 hPa pressure level).

Mineral dust is prognostically calculated. Dust emission fluxes are parameterized based on the 10-m wind speed and include particle sizes ranging from 0.2 to 1,300 μm. The mass flux is then transferred into two particle size distributions (accumulation and coarse mode), which are assumed to be log-normal. Aerosol dynamics considers microphysical processes such as coagulation, in- and below cloud scavenging (wet deposition), turbulent (dry) deposition and gravitational settling (Stier et al., 2005).

The novelty of the model setup is the fully interactive coupling between dust emissions and the dynamic land surface and vegetation model JSBACH, which is an integral part of ECHAM6 (Reick et al., 2013; Stevens et al., 2013). Instead of prescribing a source file, the emissions are calculated for each (land) grid cell in each time step. Each grid cell is assumed to be tiled, allowing various shares of soil and 12 different plant functional types. The soil types for each region are described in Tegen et al. (2002) and consist of varying proportions of coarse sand, fine sand, silt and clay. Dust sources are based on a scheme by Stanelle et al. (2014), where terrestrial tiles not covered by vegetation represent potential dust sources and tiles covered by snow or vegetation block dust emissions. While gaps in low-stature vegetation (shrubs and crops) allow for dust emissions, gaps in forests prevent them. This dynamic simulation of vegetation and thus the size of dust emission areas is a next step toward a fully interactive coupling between global climate and the mineral dust cycle.

3. Results and Discussion

3.1. Sediment Grain Size and End Members

The grain-size distributions of the South Atlantic surface sediments show a wide variety of poorly sorted sediments. Most samples show polymodal grain-size distributions and are likely composed of multiple different base components (Figure 2a). Modal grain sizes range from 1.5 to 127.6 μm. Samples from nearly the same location (within a maximum radius of 55 km) show very consistent grain-size distributions (Figure 2b). Some of the observed transects (Figure 2c) show the input of locally derived sediments or IRD. The Scotia Sea transect shows nearly identical grain-size distributions again except for the southernmost sample, which is close to the South Orkney Islands in the Southern Ocean, and therefore likely containing additional sediments than mineral dust only. The two Antarctic transects show a northward fining, reflecting the input of IRD from the Antarctic continent. Overall, the four EMs describe the variability of the original data set well (Figure 3).

The most important dust source in the South Atlantic is South America (Krätschmer, van der Does, et al., 2022; Neff & Bertler, 2015). Dust collected at multiple sites in Patagonia with horizontal Big Spring Number Eight (BSNE) samplers (representing dust in transport toward the ocean) reveals a finest EM with modal grain sizes of 10–17 μm, and a coarser EM of approximately 30–50 μm (Cosentino et al., 2021). This is in line with dust collected at a monitoring station at the core of the loessic Pampean plains, Argentina, which shows a dominant modal grain size and EM of 12 μm and a coarser EM with a mode of 30–40 μm (Cosentino et al., 2020). The former corresponds to the finer mode of various source sediments for the northern Puna (11.6 μm), southern Puna (8.8 μm), southern Altiplano (15.2 μm) and the shores of Mar Chiquita Lake in Central Argentina (17.4 μm). The finest EM they observed (6–8 μm) is interpreted to be the result of long-range dust transport (Cosentino et al., 2020). This also agrees with EM reconstructions from Pampean Plain loess samples (Torre et al., 2020). These findings correspond well to EM1 and EM2 found for the Atlantic surface sediments, although these are finer grained due to the longer transport distance across the ocean. EM1 and EM2 are also similar to dust grain-size distributions in the South Atlantic (ODP Site 1090) and South Pacific (PS75/056-1), which have modal grain sizes of 2.7 μm (0–1 cm bsf) and 3.7 μm (7–8 cm bsf), identical to their long-term averages of 160,000 and 260,000 years, respectively (van der Does, Wengler, et al., 2021).

Riverine and hemipelagic sediments sampled close to continental shores are often found to be finer-grained components of deep-sea sediments than aeolian dust (Holz et al., 2004; Stuut et al., 2002; Stuut & Lamy, 2004). In our study, this is largely avoided due to the location of the sediment samples >300 km from the African and South American coasts. In places at large distances from the sediment sources, it was found that (long-range) aeolian dust can be finer-grained than hemipelagic sediments (e.g., Rea & Hovan, 1995). Therefore, EM2 and EM1 are considered to represent coarser-grained and finer-grained dust components, respectively. These two dust components could potentially be related to the atmospherically traveled distance, with coarser-grained dust deposited closer to the dust sources, and finer-grained dust transported over greater distances (van der Does et al., 2016). EM1 is also comparable to long-range dust transport to Antarctica, which typically shows modal grain sizes of ~2 μm, with maximum particle diameters of approximately 5 μm (Delmonte et al., 2020). Possible contributions from riverine sediments could still be represented in the two dust EMs, especially at the site close to the continents and major rivers (Figure 2).

Present-day dust collected directly from the atmosphere over the course of several hours to days off the Namibian coast (Stuut et al., 2002) and Angola (Stuut et al., 2005) is, with modal grain sizes of about 20 and 30 μm, coarser-grained than the two dust end members EM1 and EM2. However, seafloor surface sediments are generally finer grained than aerosol samples from the same location (Stuut et al., 2005; van der Does, Brummer, et al., 2021). This is due to the short time span aerosol samples represent and are therefore susceptible to short-term meteorological conditions compared to seafloor sediments that can span several hundreds of years per centimeter.

EM3 has a clear (bottom)current-driven character with a modal grain size of 34.6 μm and nearly 70% of particles in the sortable silt fraction (SS; 10–63 μm). Sortable silt is sensitive to bottom-current sorting due to its non-cohesive behavior, and for that reason, it is often used as a paleocurrent indicator (McCave et al., 1995). The good relation between the SS mean grain size $\overline{SS}$ (μm) and percentage SS (%) ($R^2 = 0.79$) is an indication that the SS fraction is mainly sorted by currents (McCave & Andrews, 2019). The correlations between EM3 and $\overline{SS}$ and SS (%) are lower, with $R^2 = 0.46$ and $R^2 = 0.64$, respectively, but still give a good indication that EM3 is predominantly composed of current-sorted sediments. Generally, long-range transported dust is mostly limited to particles <30 μm (Ryder et al., 2013; van der Does et al., 2016), although sometimes coarser particles may persist (Ryder et al., 2019). Therefore, EM3 is not considered to represent an important dust fraction in the South Atlantic surface sediments, although perhaps not negligible in some areas. An alternative 5-EM scenario could possibly include a (super-)coarse dust EM. For the long-range dust transport that these samples represent, however, this would represent a very small fraction of the total dust flux. In addition, EM4 in the 5-EM scenario would in turn represent SS, showing an uncharacteristic coarse and unsorted distribution, making this scenario unlikely.

The sediments of the SS fraction alone might not be reliable for current-speed reconstructions as it is also composed of IRD and coarse dust particles. An alternative method for isolating the current-sorted sediment fraction was proposed by Stevenard et al. (2023) using a similar EM modeling approach, except with a higher number of end members. However, mineral dust has generally overlapping grain sizes with SS, and would be contained in that fraction in areas with higher dust concentrations using their method.

IRD, which is released by icebergs, can be another potential sediment source to the South Atlantic Ocean and has a highly unsorted character (Dowdeswell, 2009; McCave & Andrews, 2019). Icebergs may drift up to thousands of kilometers from their glacial sources, which include East Antarctica, the Antarctic Peninsula, Southern Ocean Islands such as the South Sandwich Island and Bouvet Island, as well as Patagonian ice sheets during glacial periods (Diekmann et al., 2003; Nielsen et al., 2007). IRD often contains (coarse) sand particles, which are too large to be transported to the remote open ocean by bottom currents (Diekmann & Kuhn, 1999; Jonkers et al., 2015). In marine sediments, the terrigenous sand content >63 μm is often used as a proxy for IRD input. EM4 is comprised for ~46% of particles >63 μm, and the correlation between the >63 μm fraction of the samples and EM4 is very good ($R^2 = 0.98$), while the correlation between EM3 and the >63 μm fraction is zero. Therefore, EM4 is considered to represent the IRD fraction in the sediments, and close to landmasses these coarse particles can also be supplied directly by debris flows.

The contributions of each EM to the South Atlantic yield important information (Figure 4), although these are only relative values and not absolute fluxes. The two dust end members EM1 and EM2 make up the majority over the central south Atlantic, and the coarser-grained end members have a relatively larger contribution close to the coasts. EM4, which is considered to represent IRD, is only observed north of Antarctica up to approximately 50°
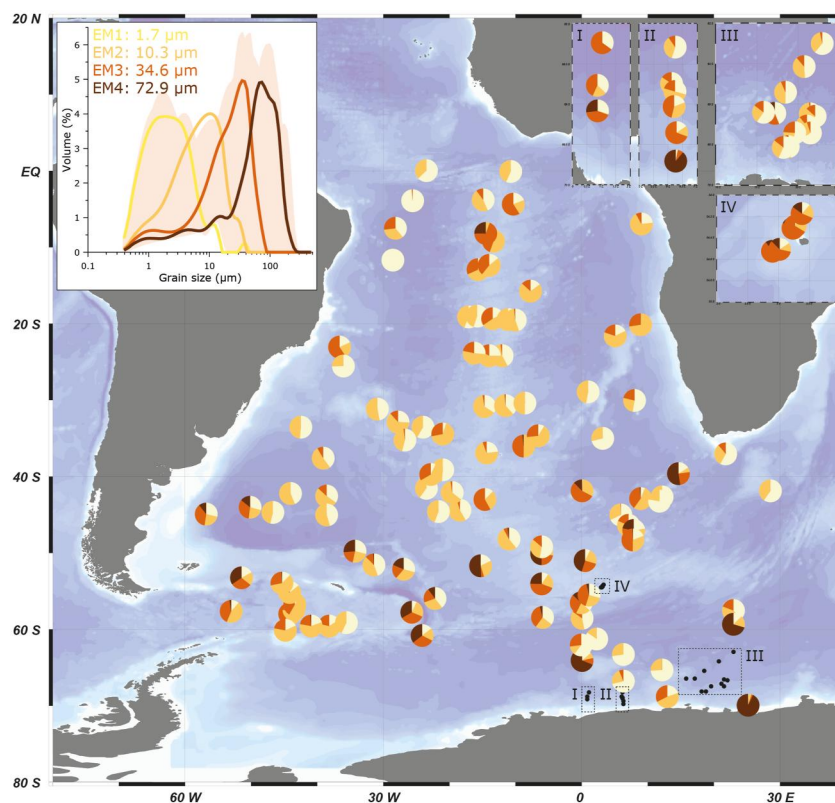
Figure 4. Grain-size distributions of the four EMs (lines), with the range of grain-size distributions of the original data set (shaded area; both top left insert), and the relative contributions (%) of each end-member to the total grain-size distributions of the samples (map and top right inserts, N = 128). The map was generated using Ocean Data View (Schlitzer, 2018).

S. This is consistent with previous observations of icebergs in the South Atlantic up to 50°S, much further north than the maximum sea ice limit (Kienast et al., 2016; Tournadre et al., 2012), therefore confirming the ice-rafted origin of EM4. Absolute fluxes of the four different end members would provide more information on the distribution of the different sediment components over the South Atlantic Ocean.

3.2. Lithogenic Fluxes

The lithogenic fluxes comprise all lithogenic components, including mineral dust, as well as current-transported sediments and IRD. These are shown in Figure 5 as an interpolated background, using Data Interpolating Variational Analysis (DIVA; Troupin et al., 2012) with Ocean Data View (Schlitzer, 2018), which is an interpolation method that also takes into account coastlines and bathymetry features for structuring and subdividing the domain.

Due to a process called boundary scavenging, an offset between the ^{230}Th burial flux and its overlying production can exist. Simulations with a general circulation model with a simple particle-flux module suggested that 70% of the ocean floor receives a flux within 30% of that expected from the overlying production in the water column (Costa et al., 2020; Henderson et al., 1999). However, these uncertainties related to the transport of Thorium fluxes to the ocean floor are not incorporated into the uncertainties of the flux calculations, which only consider the analytical errors.

The highest lithogenic fluxes are concentrated around the continental margins, and only little lithogenic material reaches the remote open ocean (Figure 5). These fluxes and their absolute values are very similar to published ^{230}Th-normalized lithogenic fluxes of the Holocene (Kohfeld et al., 2013; Ouyang et al., 2021). In the Weddell Sea, where no surface sediments were analyzed, the published data show relatively high lithogenic fluxes.
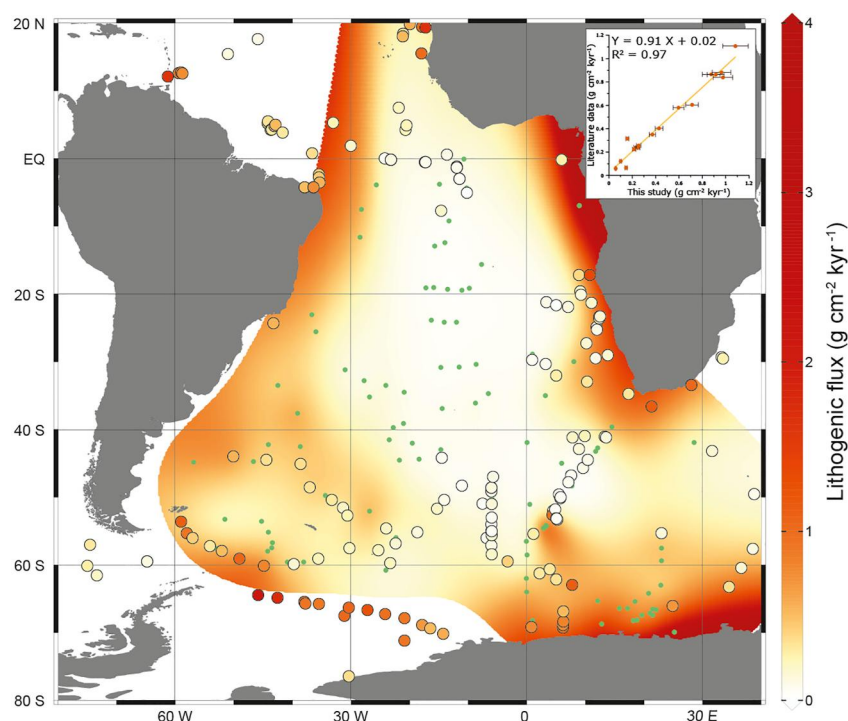
Figure 5. Lithogenic fluxes in the South Atlantic. Interpolated (Data Interpolating Variational Analysis, or DIVA) background: results from this study (sample locations in green points, $N = 128$). Circles: lithogenic fluxes from Kohfeld et al. (2013) and Ouyang et al. (2021). Top-right insert: comparison between lithogenic fluxes from this study (with 1σ error bars) and the literature data (no errors available) from identical stations ($N = 17$). The map was generated using Ocean Data View (Schlitzer, 2018).

Off southern South America, the main source of lithogenic material is mineral dust (Figure 4). As a result, the lithogenic fluxes decrease downwind, as increasingly more dust settles along its trajectory during transport. Off Antarctica, increased fluxes likely result from lithogenic particles transported by icebergs and meltwater runoff from the continent. The high flux off western Africa is the result of a single sample, and is likely riverine runoff from the Congo River.

Many studies often regard the lithogenic flux in remote locations as solely composed of dust. Here, we quantify the dust flux more specifically and accurately by using an EM-defined dust fraction.

3.3. Sediment Components in the South Atlantic

Since the data presented here cover a vast area of the globe, and the samples are complex mixtures of different sediment types (mineral dust, hemipelagic, riverine and current-sorted sediments, IRD), different sources of said sediment types with different signatures and characteristics, as well as sorting processes during transport and deposition, unmixing these is challenging and comes with certain limitations. Especially, close to the Antarctic continent, the sediment input is found to be more difficult to discriminate. Therefore, all samples within the Antarctic Circle (66.5°S, or approximately <300 km from the Antarctic continent) were excluded from the determination of specific sediment fluxes ($N = 18$). For the initial sample selection, samples <300 km from the African and South American coasts were already rejected to avoid hemipelagic and riverine sediment input (after the strategy outlined by Kienast et al., 2016), which is now also applied to the Antarctic coast. Riverine sediments are difficult to separate from mineral dust in our 4EM model, since their grain sizes overlap and no dedicated EM for riverine sediments was reconstructed. Samples with a large 1σ relative uncertainty were additionally removed (>10%, $N = 7$), resulting in a filtered data set of 103 samples considered for the specific flux determination.

After having defined the dust fraction in the sediments (EM1 + EM2), multiplying this with the Th lithogenic fluxes will result in absolute dust fluxes in the South Atlantic Ocean, as well as the current-sorted (EM3) and IRD (EM4) fluxes (Figure 6). A similar method was applied by McGee et al. (2013) for down-core aeolian-dust
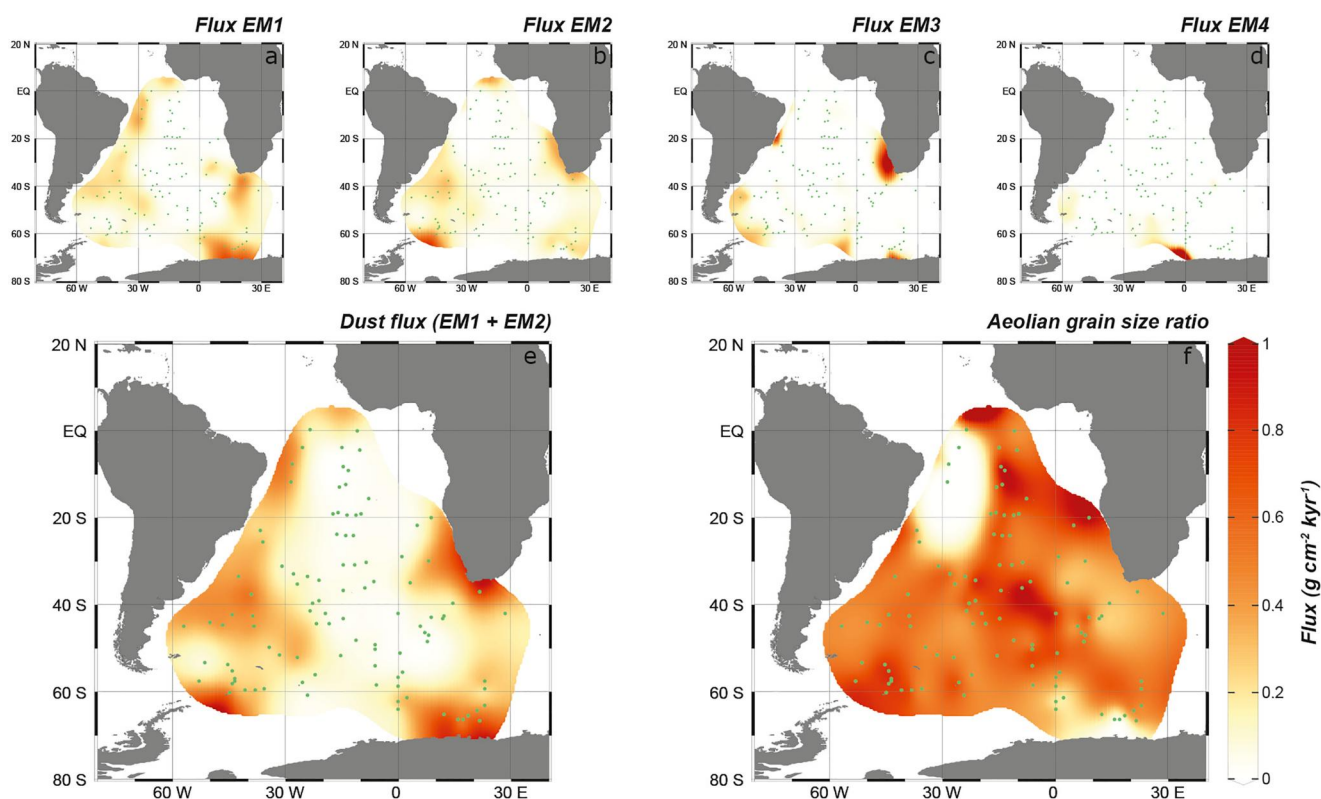
Figure 6. Sediment fluxes (g cm^{-2} Kyr^{-1}) for the four individual end-members in the South Atlantic Ocean (a–d), dust flux (e; defined as EM1 + EM2) and the aeolian grain size ratio (f; defined as the ratio of the coarse over the fine dust end member EM2/(EM2 + EM1)), interpolated using Data Interpolating Variational Analysis (DIVA). Exact sample locations are marked with green points. Each graph uses the same color scale. $N = 103$, after additional filtering (see text). The maps were generated using Ocean Data View (Schlitzer, 2018).

records off northwest Africa. The ratio of the coarse over the fine dust end member (EM2/(EM2 + EM1); Figure 6f) reflects the aeolian grain size ratio. For down-core records this is usually interpreted as a proxy for wind strength (Stuut et al., 2002). Here, we interpret the aeolian grain size ratio as a measure for the traveled distance, or the distance to the dust source. Higher values mean coarser-grained dust, and therefore closer to the dust source as these are deposited earlier, and finer-grained particles are transported over greater distances. The aeolian grain size might in some locations also be partly influenced by precipitation, where especially below-cloud scavenging favors the deposition of coarse-grained particles (Bergametti & Forêt, 2014; van der Does, Brummer, et al., 2021). However, it is difficult to identify such processes from the presented samples, that represent several hundreds of years of dust deposition, and therefore variable precipitation patterns.

Dust fluxes in the South Atlantic range between 0 and 0.84 g cm^{-2} Kyr^{-1} (Figure 6e). The dust fraction shows increased fluxes off southern South America (up to 0.71 g cm^{-2} Kyr^{-1}), the main dust source to the South Atlantic Ocean, and a clear decrease downwind as a result of dust settling into the ocean. Satellite images of modern dust deposition show a similar SE transport pathway as the decrease in dust flux (Figure 1). The expected downwind fining of the aeolian grain size ratio is not clear (Figure 6f). However, both individual dust end members sharply decrease downwind (Figures 6a and 6b), with only very low fluxes in the remote open ocean. As they decrease at almost the same rate, this results in little variation of the aeolian grain size ratio, demonstrating that the fine dust end member (EM1) is not simply a background component deposited over the entire South Atlantic but also has a clear track downwind of its South American and southern African sources. The coarse dust end member (EM2) is primarily focused on the prominent South American sources. Dust fluxes are also increased off southern Africa, close to prominent dust sources. This dust is transported by less-efficient dust-transporting winds, and therefore does not reach as far south as South American dust. The aeolian grain size ratio further displays areas with increased values in the central South Atlantic, which might be the result of reworking of sediments, or current transport. However, these values might not be very representative, since the total lithogenic flux and dust flux are
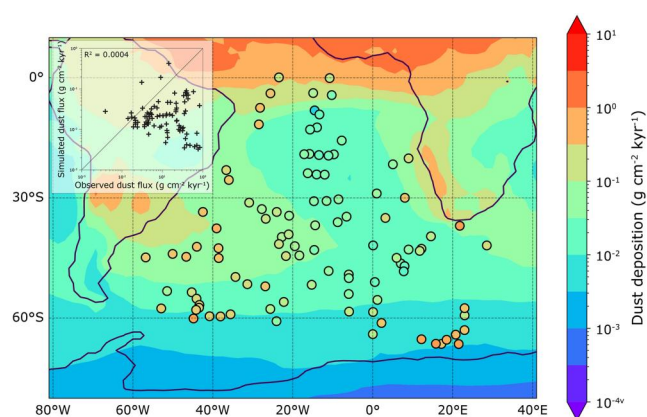
Figure 7. Simulated (background, Late Holocene) and observed (circles; defined as EM1 + EM2) dust deposition fluxes over the South Atlantic Ocean. The top-left insert shows the relation between the observed and simulated dust fluxes.

very low in these remote locations. Just off the coast of Namibia, a single sample shows a high aeolian grain size ratio (since EM2 contributes 100% to the dust fraction of this sample), meaning that the dust potentially originates from proximal sources in southern Africa. However, their contributions are relatively small, since the total dust flux is low (0.20 g cm^{-2} Kyr^{-1}). Dupont and Wyputta ([2003](#)) attribute this to unfavorable winds for dust transport out of Africa.

Dust fluxes seem to be strongly increased just off Antarctica (up to 0.84 g cm^{-2} Kyr^{-1}). Although all samples within the Antarctic Circle (66.5° S) were removed from the specific-flux determination, these samples are likely still influenced by (fine-grained) IRD input or current-sorted sediments. This is also indicated by the increased IRD (EM4) and SS (EM3) fractions, and because this area is not a prominent sink for increased fluxes of long-range wind-blown dust. These may also have overlapping grain size with the dust fraction (Stevenard et al., [2023](#)), which the EM modeling did not separate completely. However, some local dust sources exist in Antarctica (Meinander et al., [2022](#)), although these are more likely to supply coarser-grained particles than EM1 and EM2 due to their proximity. The IRD flux

reaches values up to 3.6 g cm^{-2} Kyr^{-1} for the unfiltered samples and decreases northward until it is virtually absent north of 50°S. IRD mainly contributes to the sediments on the Antarctic shelf but is a minor source of deep-sea sediments (Petschick et al., [1996](#)). In addition to IRD transported by Antarctic ice bergs, it can also be transported by icebergs from the Antarctic and sub-Antarctic islands, and possibly (glacial) Patagonia (Bigg, [2020](#)), explaining increased fluxes of EM4 (and EM3) around the (sub)Antarctic islands in the Southern Ocean.

Another interesting feature that can be seen in the dust fluxes over the South Atlantic Ocean is an increased dust flux northeast of South America, mostly the result of high EM1 fluxes. Here, the aeolian grain size ratio is small, indicating that the dust is deposited far from its source. It is therefore very likely that this dust is transported from Northern Hemisphere dust sources, such as the southern regions of the Sahara Desert in northern Africa. Transport across the equator from the sources has been observed previously but has been found to be limited due to low latitudinal wind speeds and high (wet) deposition around the equator (Lamancusa & Wagstrom, [2019](#)).

The flux of EM3, which represents current-transported sediments, has a close similarity to concentrations of particulate matter just above the seafloor from nepheloid layers (Gardner et al., [2018](#)). These nepheloid layers are the result of increased (bottom) current velocities, and are concentrated around the continental margins. Like the dust fraction, EM3 shows increased fluxes off southern South America, although these represent only a few single samples and are mostly close to the South American coast. Close to the Antarctic Peninsula and off the Antarctic coast, EM3 is also increased, where the dust fraction is also higher. The aeolian grain size ratio, however, is large, indicating local sources, which would be in line with increased IRD input instead of mineral dust.

3.4. Comparison to Model Simulations

Since direct observations of dust deposition in the remote open ocean are difficult to obtain, many studies aim at bridging that gap with model simulations of global dust deposition (e.g., Albani et al., [2016](#); Kok et al., [2021a](#); Mahowald et al., [2014](#)). These do not always produce dust fluxes that are in line with direct observations, which are the result of for example, incorrect characterization of coarse dust particles (Adebiyi & Kok, [2020](#)) or sea surface temperatures (Krätschmer, Cauquoin, et al., [2022](#)).

When comparing new model simulations of dust deposition over the South Atlantic Ocean from Krätschmer, van der Does, et al. ([2022](#)) to our EM-defined dust fluxes, there are clear similarities (Figure [7](#)). First, the order of magnitude of the deposition fluxes compares very well, although the observed dust fluxes are systematically higher. Both data sets show a prominent dust plume coming from South America that decreases downwind. Interhemispheric dust transport from the Sahara Desert is also reflected in the model simulations, although with lower fluxes than the observed data in the western equatorial Atlantic, and higher simulated fluxes in the central equatorial Atlantic. In the remote open ocean, both simulated and observed dust fluxes are low. The increased dust fluxes off Antarctica of the observed data are not reflected by the model simulations. This supports the

explanation that these increased fluxes are locally derived sediments and IRD, and not dust deposition. The resulting correlation between observed and simulated fluxes is very low due to these mentioned discrepancies ($R^2 = 0.0004$).

The match between direct observations and model simulations of dust deposition off the main sources in South America and southern Africa, both independent approaches to a hard-to-study phenomenon, highlights the importance of this data set. Observations like the ones presented here are important to validate and calibrate model simulations. The model simulations can in turn provide a wider geographical coverage for remote areas and can provide additional context to observed fluxes or anomalies.

4. Conclusions

We have studied an extensive set of samples covering the entire South Atlantic Ocean for dust grain-size and fluxes. By using EM modeling, we aimed to disentangle the polymodal grain-size distributions into a fine and coarse dust components, as well as current-sorted sediments and IRD. These were combined with ^{230}Th-normalized lithogenic fluxes to quantify the specific fluxes for these four lithogenic end members. The dust fluxes are generally found to be lower than published records and global compilations of lithogenic fluxes to the remote open ocean, due to the assumption that all pelagic fluxes are mineral dust. We conclude that dust fluxes characterized by EM modeling are a major step in order to better quantify modern and past dust input to the ocean.

In general, the new dust flux estimates are highest off the major sources off southern South America and southern Africa, and decrease downwind. In some places, the dust fluxes appear to be influenced by fine-grained IRD or riverine sediments, which may have overlapping grain sizes. However, in dust-dominated areas, the dust fluxes seem very accurate. Therefore, when interpreting these specific dust fluxes, their location and sedimentological context need to be carefully considered. The aeolian grain size ratio (the ratio of the coarse over the fine dust EM) gives additional information on the traveled distance of dust particles and reveals input from Northern Hemisphere dust sources to the South Atlantic. The observations show apparent similarities to independent model-based dust fluxes over the South Atlantic Ocean, and these can complement each other for validation and reconstruction of dust deposition in remote areas.

Data Availability Statement

Data used in this manuscript are stored at https://doi.org/10.1594/PANGAEA.961706 (van der Does et al., 2023).

References

Adebiyi, A. A., & Kok, J. F. (2020). Climate models miss most of the coarse dust in the atmosphere. *Science Advances*, *6*(15), eaaz9507. https://doi.org/10.1126/sciadv.aaz9507

Albani, S., Mahowald, N. M., Murphy, L. N., Raiswell, R., Moore, J. K., Anderson, R. F., et al. (2016). Paleodust variability since the Last Glacial Maximum and implications for iron inputs to the ocean. *Geophysical Research Letters*, *43*(8), 3944–3954. https://doi.org/10.1002/2016gl067911

Arimoto, R. (2001). Eolian dust and climate: Relationships to sources, tropospheric chemistry, transport and deposition. *Earth-Science Reviews*, *54*(1), 29–42. https://doi.org/10.1016/S0012-8252(01)00040-X

Bacon, M. P. (1984). Glacial to interglacial changes in carbonate and clay sedimentation in the Atlantic Ocean estimated from ^{230}Th measurements. *Chemical Geology*, *46*(2), 97–111. https://doi.org/10.1016/0009-2541(84)90183-9

Bergametti, G., & Forêt, G. (2014). Dust deposition. In P. Knippertz & J. B. W. Stuut (Eds.), *Mineral dust, A key player in the Earth system* (pp. 179–200). Springer Science+Business Media, Springer. https://doi.org/10.1007/978-94-017-8978-3

Bigg, G. R. (2020). The impact of icebergs of sub-Antarctic origin on Southern Ocean ice-rafted debris distributions. *Quaternary Science Reviews*, *232*, 106204. https://doi.org/10.1016/j.quascirev.2020.106204

Cheng, H., Lawrence Edwards, R., Shen, C.-C., Polyak, V. J., Asmerom, Y., Woodhead, J., et al. (2013). Improvements in ^{230}Th dating, ^{230}Th and ^{234}U half-life values, and U–Th isotopic measurements by multi-collector inductively coupled plasma mass spectrometry. *Earth and Planetary Science Letters*, *371–372*, 82–91. https://doi.org/10.1016/j.epsl.2013.04.006

Comiso, J. C. (2003). Warming trends in the Arctic from clear sky satellite observations. *Journal of Climate*, *16*(21), 3498–3510. https://doi.org/10.1175/1520-0442(2003)016<3498:Wtitaf>2.0.Co;2

Cosentino, N. J., Gaiero, D. M., & Lambert, F. (2021). Present-day patagonian dust emissions: Combining surface visibility, mass flux, and reanalysis data. *Journal of Geophysical Research: Atmospheres*, *126*(16), e2020JD034459. https://doi.org/10.1029/2020JD034459

Cosentino, N. J., Gaiero, D. M., Torre, G., Pasquini, A. I., Coppo, R., Arce, J. M., & Vélez, G. (2020). Atmospheric dust dynamics in southern South America: A 14-year modern dust record in the loessic Pampean region. *The Holocene*, *30*(4), 575–588. https://doi.org/10.1177/0959683619875198

Costa, K. M., Hayes, C. T., Anderson, R. F., Pavia, F. J., Bausch, A., Deng, F., et al. (2020). ^{230}Th Normalization: New insights on an essential tool for quantifying sedimentary fluxes in the Modern and Quaternary Ocean. *Paleoceanography and Paleoclimatology*, *35*(2), e2019PA003820. https://doi.org/10.1029/2019PA003820

Delmonte, B., Winton, H., Baroni, M., Baccolo, G., Hansson, M., Andersson, P., et al. (2020). Holocene dust in East Antarctica: Provenance and variability in time and space. *The Holocene*, *30*(4), 546–558. https://doi.org/10.1177/0959683619875188

Diekmann, B., Fütterer, D. K., Grobe, H., Hillenbrand, C. D., Kuhn, G., Michels, K., et al. (2003). Terrigenous sediment supply in the polar to temperate South Atlantic: Land-ocean links of environmental changes during the late Quaternary. In G. Wefer, S. Mulitza, & V. Ratmeyer (Eds.), *The South Atlantic in the late Quaternary: Reconstruction of material budget and current systems* (pp. 375–399). Springer-Verlag.

Diekmann, B., & Kuhn, G. (1999). Provenance and dispersal of glacial–marine surface sediments in the Weddell Sea and adjoining areas, Antarctica: Ice-rafting versus current transport. *Marine Geology*, *158*(1), 209–231. https://doi.org/10.1016/S0025-3227(98)00165-0

Dowdeswell, J. A. (2009). Ice-Rafted Debris (IRD). In V. Gornitz (Ed.), *Encyclopedia of paleoclimatology and ancient environments* (pp. 471–473). Springer Netherlands. https://doi.org/10.1007/978-1-4020-4411-3_113

Duce, R. A., Liss, P. S., Merrill, J. T., Atlas, E. L., Buat-Menard, P., Hicks, B. B., et al. (1991). The atmospheric input of trace species to the world ocean. *Global Biogeochemical Cycles*, *5*(3), 193–259. https://doi.org/10.1029/91GB01778

Dupont, L. M., & Wyputta, U. (2003). Reconstructing pathways of Aeolian pollen transport to the marine sediments along the coastline of SW Africa. *Quaternary Science Reviews*, *22*(2), 157–174. https://doi.org/10.1016/S0277-3791(02)00032-X

Durack, P. J., & Taylor, K. E. (2019). PCMDI AMIP SST and sea-ice boundary conditions version 1.1.6 [Dataset]. https://doi.org/10.22033/ESGF/input4MIPs.12381

Fleisher, M. Q., & Anderson, R. F. (2003). Assessing the collection efficiency of Ross Sea sediment traps using ^{230}Th and ^{231}Pa. *Deep Sea Research Part II: Topical Studies in Oceanography*, *50*(3), 693–712. https://doi.org/10.1016/S0967-0645(02)00591-X

Francois, R., Frank, M., Rutgers van der Loeff, M. M., & Bacon, M. P. (2004). ^{230}Th normalization: An essential tool for interpreting sedimentary fluxes during the late Quaternary. *Paleoceanography*, *19*(1), PA1018. https://doi.org/10.1029/2003pa000939

Gaiero, D. M., Probst, J. L., Depetris, P. J., Bidart, S. M., & Leleyter, L. (2003). Iron and other transition metals in Patagonian riverborne and windborne materials: Geochemical control and transport to the southern South Atlantic Ocean. *Geochimica et Cosmochimica Acta*, *67*(19), 3603–3623. https://doi.org/10.1016/S0016-7037(03)00211-4

Gardner, W. D., Richardson, M. J., & Mishonov, A. V. (2018). Global assessment of benthic nepheloid layers and linkage with upper ocean dynamics. *Earth and Planetary Science Letters*, *482*, 126–134. https://doi.org/10.1016/j.epsl.2017.11.008

Gassó, S., & Stein, A. F. (2007). Does dust from Patagonia reach the sub-Antarctic Atlantic Ocean? *Geophysical Research Letters*, *34*(1), L01801. https://doi.org/10.1029/2006gl027693

Gili, S., Gaiero, D. M., Goldstein, S. L., Chemale, F., Jweda, J., Kaplan, M. R., et al. (2017). Glacial/interglacial changes of Southern Hemisphere wind circulation from the geochemistry of South American dust. *Earth and Planetary Science Letters*, *469*, 98–109. https://doi.org/10.1016/j.epsl.2017.04.007

Gili, S., Vanderstraeten, A., Chaput, A., King, J., Gaiero, D. M., Delmonte, B., et al. (2022). South African dust contribution to the high southern latitudes and East Antarctica during interglacial stages. *Communications Earth & Environment*, *3*(1), 129. https://doi.org/10.1038/s43247-022-00464-z

Henderson, G. M., & Anderson, R. F. (2003). The U-series toolbox for paleoceanography. *Reviews in Mineralogy and Geochemistry*, *52*(1), 493–531. https://doi.org/10.2113/0520493

Henderson, G. M., Heinze, C., Anderson, R. F., & Winguth, A. M. E. (1999). Global distribution of the ^{230}Th flux to ocean sediments constrained by GCM modelling. *Deep Sea Research Part I: Oceanographic Research Papers*, *46*(11), 1861–1893. https://doi.org/10.1016/S0967-0637(99)00030-8

Holz, C., Stuut, J. B. W., & Henrich, R. (2004). Terrigenous sedimentation processes along the continental margin off NW Africa: Implications from grain-size analysis of seabed sediments. *Sedimentology*, *51*(5), 1145–1154. https://doi.org/10.1111/j.1365-3091.2004.00665.x

Johnson, M. S., Meskhidze, N., Solmon, F., Gassó, S., Chuang, P. Y., Gaiero, D. M., et al. (2010). Modeling dust and soluble iron deposition to the South Atlantic Ocean. *Journal of Geophysical Research*, *115*(D15), D15202. https://doi.org/10.1029/2009jd013311

Jonkers, L., Barker, S., Hall, I. R., & Prins, M. A. (2015). Correcting for the influence of ice-rafted detritus on grain size-based paleocurrent speed estimates. *Paleoceanography*, *30*(10), 1347–1357. https://doi.org/10.1002/2015pa002830

Kienast, S. S., Winckler, G., Lippold, J., Albani, S., & Mahowald, N. M. (2016). Tracing dust input to the global ocean using thorium isotopes in marine sediments: ThoroMap. *Global Biogeochemical Cycles*, *30*(10), 1526–1541. https://doi.org/10.1002/2016gb005408

Kohfeld, K. E., Graham, R. M., de Boer, A. M., Sime, L. C., Wolff, E. W., Le Quéré, C., & Bopp, L. (2013). Southern Hemisphere westerly wind changes during the Last Glacial Maximum: Paleo-data synthesis. *Quaternary Science Reviews*, *68*, 76–95. https://doi.org/10.1016/j.quascirev.2013.01.017

Kok, J. F., Adebiyi, A. A., Albani, S., Balkanski, Y., Checa-Garcia, R., Chin, M., et al. (2021a). Improved representation of the global dust cycle using observational constraints on dust properties and abundance. *Atmospheric Chemistry and Physics*, *21*(10), 8127–8167. https://doi.org/10.5194/acp-21-8127-2021

Kok, J. F., Adebiyi, A. A., Albani, S., Balkanski, Y., Checa-Garcia, R., Chin, M., et al. (2021b). Contribution of the world's main dust source regions to the global cycle of desert dust. *Atmospheric Chemistry and Physics*, *21*(10), 8169–8193. https://doi.org/10.5194/acp-21-8169-2021

Krätschmer, S., Cauquoin, A., Lohmann, G., & Werner, M. (2022). A modeling perspective on the lingering glacial sea surface temperature conundrum. *Geophysical Research Letters*, *49*(23), e2022GL100378. https://doi.org/10.1029/2022GL100378

Krätschmer, S., van der Does, M., Lamy, F., Lohmann, G., Völker, C., & Werner, M. (2022). Simulating glacial dust changes in the Southern Hemisphere using ECHAM6.3-HAM2.3. *Climate of the Past*, *18*(1), 67–87. https://doi.org/10.5194/cp-18-67-2022

Lamancusa, C., & Wagstrom, K. (2019). Global transport of dust emitted from different regions of the Sahara. *Atmospheric Environment*, *214*, 116734. https://doi.org/10.1016/j.atmosenv.2019.05.042

Lambert, F., Delmonte, B., Petit, J. R., Bigler, M., Kaufmann, P. R., Hutterli, M. A., et al. (2008). Dust-climate couplings over the past 800,000 years from the EPICA Dome C ice core. *Nature*, *452*(7187), 616–619. https://doi.org/10.1038/nature06763

Li, F., Ginoux, P., & Ramaswamy, V. (2008). Distribution, transport, and deposition of mineral dust in the Southern Ocean and Antarctica: Contribution of major sources. *Journal of Geophysical Research*, *113*(D10), D10207. https://doi.org/10.1029/2007jd009190

Mahowald, N., Albani, S., Kok, J. F., Engelstaeder, S., Scanza, R., Ward, D. S., & Flanner, M. G. (2014). The size distribution of desert dust aerosols and its impact on the Earth system. *Aeolian Research*, *15*, 53–71. https://doi.org/10.1016/j.aeolia.2013.09.002

Martin, J. H. (1990). Glacial-interglacial CO_2 change: The iron hypothesis. *Paleoceanography*, *5*(1), 1–13. https://doi.org/10.1029/PA005i001p00001

Martínez-García, A., Sigman, D. M., Ren, H., Anderson, R. F., Straub, M., Hodell, D. A., et al. (2014). Iron fertilization of the Subantarctic Ocean during the last ice age. *Science*, *343*(6177), 1347–1350. https://doi.org/10.1126/science.1246848

McCave, I. N., & Andrews, J. T. (2019). Distinguishing current effects in sediments delivered to the ocean by ice. I. Principles, methods and examples. *Quaternary Science Reviews*, *212*, 92–107. https://doi.org/10.1016/j.quascirev.2019.03.031

McCave, I. N., Manighetti, B., & Robinson, S. G. (1995). Sortable silt and fine sediment size composition slicing - Parameters for paleocurrent speed and paleoceanography. *Paleoceanography*, *10*(3), 593–610. https://doi.org/10.1029/94PA03039

McGee, D., deMenocal, P. B., Winckler, G., Stuut, J. B. W., & Bradtmiller, L. I. (2013). The magnitude, timing and abruptness of changes in North African dust deposition over the last 20,000 yr. *Earth and Planetary Science Letters*, *371*, 163–176. https://doi.org/10.1016/j.epsl.2013.03.054

McGee, D., Winckler, G., Borunda, A., Serno, S., Anderson, R. F., Recasens, C., et al. (2016). Tracking eolian dust with helium and thorium: Impacts of grain size and provenance. *Geochimica et Cosmochimica Acta*, *175*, 47–67. https://doi.org/10.1016/j.gca.2015.11.023

Meinander, O., Dagsson-Waldhauserova, P., Amosov, P., Aseyeva, E., Atkins, C., Baklanov, A., et al. (2022). Newly identified climatically and environmentally significant high-latitude dust sources. *Atmospheric Chemistry and Physics*, *22*(17), 11889–11930. https://doi.org/10.5194/acp-22-11889-2022

Neff, P. D., & Bertler, N. A. N. (2015). Trajectory modeling of modern dust transport to the Southern Ocean and Antarctica. *Journal of Geophysical Research: Atmospheres*, *120*(18), 9303–9322. https://doi.org/10.1002/2015jd023304

Nielsen, S. H. H., Hodell, D. A., Kamenov, G., Guilderson, T., & Perfit, M. R. (2007). Origin and significance of ice-rafted detritus in the Atlantic sector of the Southern Ocean. *Geochemistry, Geophysics, Geosystems*, *8*(12), Q12005. https://doi.org/10.1029/2007GC001618

Noble, T. L., Piotrowski, A. M., Robinson, L. F., McManus, J. F., Hillenbrand, C.-D., & Bory, A. J. M. (2012). Greater supply of Patagonian-sourced detritus and transport by the ACC to the Atlantic sector of the Southern Ocean during the last glacial period. *Earth and Planetary Science Letters*, *317–318*, 374–385. https://doi.org/10.1016/j.epsl.2011.10.007

Orsi, A. H., Whitworth, T., & Nowlin, W. D. (1995). On the meridional extent and fronts of the Antarctic Circumpolar Current. *Deep Sea Research Part I: Oceanographic Research Papers*, *42*(5), 641–673. https://doi.org/10.1016/0967-0637(95)00021-W

Ouyang, S., Duan, Z., Lin, W., & Luo, Y. (2021). Revisit of thorium-based dust fluxes and their implications for the iron fertilization hypothesis. *Journal of Oceanography*, *78*(1), 49–62. https://doi.org/10.1007/s10872-021-00626-1

Paterson, G. A., & Heslop, D. (2015). New methods for unmixing sediment grain size data. *Geochemistry, Geophysics, Geosystems*, *16*(12), 4494–4506. https://doi.org/10.1002/2015gc006070

Peterson, R. G., & Stramma, L. (1991). Upper-level circulation in the South Atlantic Ocean. *Progress in Oceanography*, *26*(1), 1–73. https://doi.org/10.1016/0079-6611(91)90006-8

Petschick, R., Kuhn, G., & Gingele, F. (1996). Clay mineral distribution in surface sediments of the South Atlantic: Sources, transport, and relation to oceanography. *Marine Geology*, *130*(3), 203–229. https://doi.org/10.1016/0025-3227(95)00148-4

Prospero, J. M., Ginoux, P., Torres, O., Nicholson, S. E., & Gill, T. E. (2002). Environmental characterization of global sources of atmospheric soil dust identified with the Nimbus 7 Total Ozone Mapping Spectrometer (TOMS) absorbing aerosol product. *Reviews of Geophysics*, *40*(1), 2-1–2-31. https://doi.org/10.1029/2000RG000095

Rea, D. K. (1994). The paleoclimatic record provided by eolian deposition in the deep-sea - The geologic history of wind. *Reviews of Geophysics*, *32*(2), 159–195. https://doi.org/10.1029/93RG03257

Rea, D. K. (2007). Eolian records, deep-sea sediments. In S. A. Elias (Ed.), *Encyclopedia of Quaternary science* (pp. 643–650). Roayl Holloway, University of London, Elsevier.

Rea, D. K., & Hovan, S. A. (1995). Grain size distribution and depositional processes of the mineral component of abyssal sediments: Lessons from the North Pacific. *Paleoceanography*, *10*(2), 251–258. https://doi.org/10.1029/94PA03355

Reick, C. H., Raddatz, T., Brovkin, V., & Gayler, V. (2013). Representation of natural and anthropogenic land cover change in MPI-ESM. *Journal of Advances in Modeling Earth Systems*, *5*(3), 459–482. https://doi.org/10.1002/jame.20022

Ryder, C. L., Highwood, E. J., Lai, T. M., Sodemann, H., & Marsham, J. H. (2013). Impact of atmospheric transport on the evolution of microphysical and optical properties of Saharan dust. *Geophysical Research Letters*, *40*(10), 2433–2438. https://doi.org/10.1002/grl.50482

Ryder, C. L., Highwood, E. J., Walser, A., Seibert, P., Philipp, A., & Weinzierl, B. (2019). Coarse and giant particles are ubiquitous in Saharan dust export regions and are radiatively significant over the Sahara. *Atmospheric Chemistry and Physics*, *19*(24), 15353–15376. https://doi.org/10.5194/acp-19-15353-2019

Schlitzer, R. (2018). Ocean data view. Retrieved from https://odv.awi.de

Shao, Y. P., Wyrwoll, K. H., Chappell, A., Huang, J. P., Lin, Z. H., McTainsh, G. H., et al. (2011). Dust cycle: An emerging core theme in Earth system science. *Aeolian Research*, *2*(4), 181–204. https://doi.org/10.1016/j.aeolia.2011.02.001

Shi, N., Schneider, R., Beug, H.-J., & Dupont, L. M. (2001). Southeast trade wind variations during the last 135 kyr: Evidence from pollen spectra in eastern South Atlantic sediments. *Earth and Planetary Science Letters*, *187*(3), 311–321. https://doi.org/10.1016/S0012-821X(01)00267-9

Stanelle, T., Bey, I., Raddatz, T., Reick, C., & Tegen, I. (2014). Anthropogenically induced changes in twentieth century mineral dust burden and the associated impact on radiative forcing. *Journal of Geophysical Research: Atmospheres*, *119*(23), 13526–13546. https://doi.org/10.1002/2014JD022062

Stevenard, N., Govin, A., Kissel, C., & Van Toer, A. (2023). Correction of the IRD influence for paleo-current flow speed reconstructions in hemipelagic sediments. *Paleoceanography and Paleoclimatology*, *38*(3), e2022PA004500. https://doi.org/10.1029/2022PA004500

Stevens, B., Giorgetta, M., Esch, M., Mauritsen, T., Crueger, T., Rast, S., et al. (2013). Atmospheric component of the MPI-M Earth System Model: ECHAM6. *Journal of Advances in Modeling Earth Systems*, *5*(2), 146–172. https://doi.org/10.1002/jame.20015

Stier, P., Feichter, J., Kinne, S., Kloster, S., Vignati, E., Wilson, J., et al. (2005). The aerosol-climate model ECHAM5-HAM. *Atmospheric Chemistry and Physics*, *5*(4), 1125–1156. https://doi.org/10.5194/acp-5-1125-2005

Stuut, J. B. W., & Lamy, F. (2004). Climate variability at the southern boundaries of the Namib (Southwestern Africa) and Atacama (northern Chile) coastal deserts during the last 120,000 yr. *Quaternary Research*, *62*(3), 301–309. https://doi.org/10.1016/j.yqres.2004.08.001

Stuut, J. B. W., Prins, M. A., Schneider, R. R., Weltje, G. J., Jansen, J. H. F., & Postma, G. (2002). A 300-kyr record of aridity and wind strength in southwestern Africa: Inferences from grain-size distributions of sediments on Walvis Ridge, SE Atlantic. *Marine Geology*, *180*(1–4), 221–233. https://doi.org/10.1016/S0025-3227(01)00215-8

Stuut, J. B. W., Zabel, M., Ratmeyer, V., Helmke, P., Schefuss, E., Lavik, G., & Schneider, R. (2005). Provenance of present-day eolian dust collected off NW Africa. *Journal of Geophysical Research*, *110*(D04202), 1–14. https://doi.org/10.1029/2004JD005161

Taylor, S. R., & McLennan, S. M. (1995). The geochemical evolution of the continental crust. *Reviews of Geophysics*, *33*(2), 241–265. https://doi.org/10.1029/95RG00262

Tegen, I., Harrison, S. P., Kohfeld, K., Prentice, I. C., Coe, M., & Heimann, M. (2002). Impact of vegetation and preferential source areas on global dust aerosol: Results from a model study. *Journal of Geophysical Research*, *107*(D21), AAC-14. https://doi.org/10.1029/2001jd000963

Torre, G., Gaiero, D. M., Cosentino, N. J., & Coppo, R. (2020). The paleoclimatic message from the polymodal grain-size distribution of late Pleistocene-early Holocene Pampean loess (Argentina). *Aeolian Research*, *42*, 100563. https://doi.org/10.1016/j.aeolia.2019.100563

Tournadre, J., Girard-Ardhuin, F., & Legrésy, B. (2012). Antarctic icebergs distributions, 2002–2010. *Journal of Geophysical Research*, *117*(C5), 1–15. https://doi.org/10.1029/2011jc007441

Troupin, C., Barth, A., Sirjacobs, D., Ouberdous, M., Brankart, J. M., Brasseur, P., et al. (2012). Generation of analysis and consistent error fields using the Data Interpolating Variational Analysis (DIVA). *Ocean Modelling*, *52–53*, 90–101. https://doi.org/10.1016/j.ocemod.2012.05.002

Twohy, C. H., Kreidenweis, S. M., Eidhammer, T., Browell, E. V., Heymsfield, A. J., Bansemer, A. R., et al. (2009). Saharan dust particles nucleate droplets in eastern Atlantic clouds. *Geophysical Research Letters*, *36*(1), L01807. https://doi.org/10.1029/2008GL035846

van der Does, M., Brummer, G.-J. A., Korte, L. F., & Stuut, J.-B. W. (2021). Seasonality in Saharan dust across the Atlantic Ocean: From atmospheric transport to seafloor deposition. *Journal of Geophysical Research: Atmospheres*, *126*(11), e2021JD034614. https://doi.org/10.1029/2021JD034614

van der Does, M., Korte, L. F., Munday, C. I., Brummer, G. J. A., & Stuut, J. B. W. (2016). Particle size traces modern Saharan dust transport and deposition across the equatorial North Atlantic. *Atmospheric Chemistry and Physics*, *16*(21), 13697–13710. https://doi.org/10.5194/acp-16-13697-2016

van der Does, M., Lamy, F., Krätschmer, S., Stuut, J. B. W., Völker, C., Werner, M., & Winckler, G. (2023). Grain-size distributions, End-member modelling and Th-fluxes of South Atlantic surface sediments [Dataset]. PANGAEA. https://doi.org/10.1594/PANGAEA.961706

van der Does, M., Wengler, M., Lamy, F., Martínez-García, A., Jaccard, S. L., Kuhn, G., et al. (2021). Opposite dust grain-size patterns in the Pacific and Atlantic sectors of the Southern Ocean during the last 260,000 years. *Quaternary Science Reviews*, *263*, 106978. https://doi.org/10.1016/j.quascirev.2021.106978

van Hateren, J. A., Prins, M. A., & van Balen, R. T. (2018). On the genetically meaningful decomposition of grain-size distributions: A comparison of different end-member modelling algorithms. *Sedimentary Geology*, *375*, 49–71. https://doi.org/10.1016/j.sedgeo.2017.12.003

Weltje, G. J. (1997). End-member modeling of compositional data: Numerical-statistical algorithms for solving the explicit mixing problem. *Mathematical Geology*, *29*(4), 503–549. https://doi.org/10.1007/bf02775085

Weltje, G. J., & Prins, M. A. (2007). Genetically meaningful decomposition of grain-size distributions. *Sedimentary Geology*, *202*(3), 409–424. https://doi.org/10.1016/j.sedgeo.2007.03.007

Winckler, G., Anderson, R. F., Fleisher, M. Q., McGee, D., & Mahowald, N. (2008). Covariant glacial-interglacial dust fluxes in the equatorial Pacific and Antarctica. *Science*, *320*(5872), 93–96. https://doi.org/10.1126/science.1150595

Winckler, G., Anderson, R. F., Jaccard, S. L., & Marcantonio, F. (2016). Ocean dynamics, not dust, have controlled equatorial Pacific productivity over the past 500,000 years. *Proceedings of the National Academy of Sciences*, *113*(22), 6119–6124. https://doi.org/10.1073/pnas.1600616113